Peridynamics for multiscale materials modeling

E Askari[1], F Bobaru[2], R B Lehoucq[3], M L Parks[4], S A Silling[5], O Weckner[6]

[1,6] Applied Math, The Boeing Company, P.O. Box 3707 MC 7L-25, Seattle, WA 98124, USA
[2] Department of Engineering Mechanics, University of Nebraska-Lincoln, Lincoln, NE, 68588-0526, USA
[3,4] Applied Mathematics and Applications, Sandia National Laboratories[7], P.O. Box 5800, MS 1320, Albuquerque, NM 87185, USA
[5] Multiscale Dynamic Materials Modeling, Sandia National Laboratories, P.O. Box 5800, MS 1322, Albuquerque, NM 87185, USA

E-mail:
abe.askari@boeing.com,fbobaru2@unl.edu,rblehou@sandia.gov,mlparks@sandia.gov, sasilli@sandia.gov,olaf.weckner@boeing.com

Abstract. The paper presents an overview of peridynamics, a continuum theory that employs a nonlocal model of force interaction. This is accomplished by replacing the stress/strain relationship of classical elasticity by an integral operator that sums internal forces separated by a finite distance. This integral operator is not a function of the deformation gradient allowing for a more general notion of deformation than in classical elasticity that is well aligned with the kinematic assumptions of molecular dynamics. Peridynamics effectiveness has been demonstrated in several applications, including fracture and failure of composites, nanofiber networks, and polycrystal fracture. This suggests that peridynamics is a viable multiscale material model for length scales ranging from molecular dynamics to those of classical elasticity.

1. Introduction

The response of materials to the environments and loads occurring in practice all require an understanding of mechanics at disparate spatial and temporal scales. Such "multiscale" understanding is a fundamental challenge for next generation materials modeling, see [1] for information and references to the existing literature. A currently popular multiscale approach couples two or more well-known models, e.g., molecular dynamics and classical elasticity [2], each of which is useful at different scales. An alternative approach is to develop a single multiscale material model that remains valid and useful over a wide range of temporal and spatial scales.

The onerous practical limitations of molecular dynamics and the limited validity of classical elasticity has lead to generalized continuum theories purporting to supply a single multiscale material model. Such theories are motivated by introducing a length-scale absent in classical elasticity. These generalized continua are certainly not new; see [3, 4, 5] for overviews and citations to the abundant literature. However, these theories develop material models with a length-scale dependence by augmenting the displacement field with supplementary fields

[7] Sandia is a multiprogram laboratory operated by Sandia Corporation, a Lockheed Martin Company, for the United States Department of Energy under contract DE-AC04-94AL85000.

(e.g., rotations) that provide information about fine-scale kinematics, or by using higher-order gradients of the displacement field, or by averaging local strains and/or stresses.

This paper presents an overview of peridynamics [6, 7], a generalized continuum theory that employs a nonlocal model of force interaction. This is accomplished by replacing the stress/strain relationship of classical elasticity by an integral operator that sums internal forces separated by a finite distance. This integral operator is not a function of the deformation gradient allowing for a more general notion of deformation than classical elasticity that is well aligned with the kinematic assumptions of molecular dynamics.

2. Peridynamic primer

This section reviews peridynamic fundamentals including kinematics, balance of angular and linear momentum, length-scale, a relationship with Newtonian mechanics, and discretization. We refer the reader to [8] demonstrating that linearized peridynamics can reproduce nonlinear dispersion relationships for short wavelengths, in contrast to linear elasticity.

2.1. Kinematics and internal force density

The spatial point $\mathbf{y}$ (in the deformed configuration) is related to the material point $\mathbf{x}$ (in the reference configuration) via $\mathbf{y}(\mathbf{x},t) = \mathbf{x}+\mathbf{u}(\mathbf{x},t)$ where $\mathbf{u}(\mathbf{x},t)$ is the displacement of $\mathbf{x} \in \mathcal{B} \subset \mathbb{R}^3$. We say the body $\mathcal{B}$ undergoes deformation if the displacement $\mathbf{u}(\mathbf{x},t)$ is nonzero for some $\mathbf{x} \in \mathcal{B}$. Deformation represents the mechanism through which continuum mechanics relates deformation to the internal forces of a body. Classical elasticity assumes that the displacement field is continuously differentiable at every $\mathbf{x} \in \mathcal{B}$ so that

$$\mathbf{u}(\mathbf{x}',t) - \mathbf{u}(\mathbf{x},t) = \nabla_{\mathbf{x}}\mathbf{u}(\mathbf{x},t)(\mathbf{x}'-\mathbf{x}) + O(\|\mathbf{x}'-\mathbf{x}\|^2),$$

where $\nabla_{\mathbf{x}}$ denotes the gradient operator with respect to the material point $\mathbf{x}$. If $\mathbf{F}(\mathbf{x},t) := \mathbf{I} + \nabla_{\mathbf{x}}\mathbf{u}(\mathbf{x},t)$ denotes the deformation gradient, then

$$\mathbf{y}(\mathbf{x}',t) - \mathbf{y}(\mathbf{x},t) \approx \mathbf{F}(\mathbf{x},t)(\mathbf{x}'-\mathbf{x}).$$

In words, the body deformation $\mathbf{y}(\mathbf{x}',t) - \mathbf{y}(\mathbf{x},t)$ can be *approximated* by the deformation gradient acting on the *bond* $\mathbf{x}'-\mathbf{x}$. By relying on the true deformation $\mathbf{y}(\mathbf{x}',t) - \mathbf{y}(\mathbf{x},t)$, peridynamics avoids assumptions on the smoothness of the displacement field, in contrast to classical elasticity. The mapping from a bond $\mathbf{x}'-\mathbf{x}$ to $\mathbf{y}(\mathbf{x}',t) - \mathbf{y}(\mathbf{x},t)$, or equivalently $\mathbf{u}(\mathbf{x}',t) - \mathbf{u}(\mathbf{x},t)$, is in general nonlinear. The use of the deformation gradient is tantamount to approximating this nonlinear map with a local linear approximation.

Denote by $\mathbf{y}', \mathbf{y}$ the values $\mathbf{y}(\mathbf{x}',t), \mathbf{y}(\mathbf{x},t)$, respectively, and consider the integral operator

$$\int_{\mathcal{B}} \mathbf{k}\left(\mathbf{y}'-\mathbf{y},\mathbf{x}',\mathbf{x}\right)\, d\mathbf{x}' \tag{1}$$

representing the (internal) force density. The integral operator is nonlocal because material points $\mathbf{x}' \neq \mathbf{x}$ are involved. The constitutive equation relating deformation to internal force density is contained in the kernel $\mathbf{k}$ that has units of force per volume squared. As an example, consider a proportional microelastic material [9] with the peridynamics kernel (derivable from a stored energy function)

$$\mathbf{k}\left(\mathbf{y}'-\mathbf{y},\mathbf{x}',\mathbf{x}\right) = cs\frac{\mathbf{y}'-\mathbf{y}}{\|\mathbf{y}'-\mathbf{y}\|}, \quad s = \frac{\|\mathbf{y}'-\mathbf{y}\| - \|\mathbf{x}'-\mathbf{x}\|}{\|\mathbf{x}'-\mathbf{x}\|} \tag{2}$$

where $c/\|\mathbf{x}'-\mathbf{x}\| > 0$ is the stiffness per unit volume squared. The corresponding force density operator of classical elasticity is given by

$$\mathbf{C}(\mathbf{x},t) := \nabla_{\mathbf{x}} \cdot \mathbf{P}\left(\mathbf{F}(\mathbf{x},t)\right) \tag{3}$$

where $\mathbf{P}$ denotes the Piola-Kirchoff stress tensor and $\nabla_{\mathbf{x}}\cdot$ the divergence with respect to $\mathbf{x}$. The operator $\mathbf{C}$ is local because its value at a point $\mathbf{x}$ depends, via the deformation gradient, only on the value of the stress tensor at that same point. The Piola-Kirchoff stress tensor is a constitutive equation, e.g. a mapping from strain to stress tensors incorporating the material behavior.

The peridynamics force density operator (1) obviates the need for the stress/strain relationship implicit in (3). Such relationships are based on the idea of contact forces (interactions between material in direct contact) and follow from Cauchy's postulate [10, pp. 60–61]. Peridynamics is fundamentally different in that material separated by a finite distance may exert forces on each other. The paper [11] establishes conditions under which a peridynamic stress tensor $\boldsymbol{\nu}(\mathbf{x},t)$ exists such that

$$\nabla_{\mathbf{x}}\cdot\boldsymbol{\nu}(\mathbf{x},t)=\int_{\mathcal{B}}\mathbf{k}\left(\mathbf{y}'-\mathbf{y},\mathbf{x}',\mathbf{x}\right)\,d\mathbf{x}'.$$

But even in this case, peridynamics is fundamentally different from classical elasticity in that the peridynamics stress tensor represents a sum of forces per unit area *through* $\mathbf{x}$ instead of *at* $\mathbf{x}$, as is the case for the Piola-Kirchoff stress tensor $\mathbf{P}$.

The bond-based peridynamics model originally introduced in [6] assumed that $\mathbf{k}(\mathbf{y}'-\mathbf{y},\mathbf{x}',\mathbf{x})$ is collinear with $\mathbf{y}'-\mathbf{y}$. This assumption results in an effective Poisson ratio $=1/4$ for isotropic, linear, microelastic materials. The paper [6, § 15] also briefly described how the bond-based peridynamics kernel may be augmented so that a Poisson ratio $\neq 1/4$ can be achieved. Recently, in [7], the bond-based peridynamics model of [6] was generalized to that of a *state*-based peridynamics model for which $\mathbf{k}(\mathbf{y}'-\mathbf{y},\mathbf{x}',\mathbf{x})$ may be a force state, e.g., it may depend on the collective behavior at $\mathbf{x}$ and $\mathbf{x}'$. Peridynamics states is the continuum equivalent of the multibody potentials of classical particle mechanics that go beyond central force interactions (or the extension discussed in [6, § 15].)

2.2. Balance of linear and angular momentum

The peridynamic global balance of linear momentum is

$$\int_{\Omega}\rho(\mathbf{x})\ddot{\mathbf{u}}(\mathbf{x},t)\,d\mathbf{x}=\int_{\Omega}\int_{\mathcal{B}/\Omega}\mathbf{k}(\mathbf{y}'-\mathbf{y},\mathbf{x}',\mathbf{x})\,d\mathbf{x}'\,d\mathbf{x}+\int_{\Omega}\mathbf{b}(\mathbf{x},t)\,d\mathbf{x},\tag{4}$$

where $\rho(\mathbf{x})$ and $\mathbf{b}(\mathbf{x},t)$ are the mass and body force densities, respectively. This balance holds over any $\Omega\subset\mathcal{B}$ if and only if the peridynamic kernel is antisymmetric, e.g. $\mathbf{k}(\mathbf{y}'-\mathbf{y},\mathbf{x}',\mathbf{x})=-\mathbf{k}(\mathbf{y}-\mathbf{y}',\mathbf{x},\mathbf{x}')$. The first term on the righthand side of (4) is the analogue of the contact force in classical elasticity, and when $\Omega=\mathcal{B}$, this force is zero implying that external (to $\mathcal{B}$) contact forces play no role in peridynamics. We may define this first term to represent the force that the material in $\mathcal{B}/\Omega$ exerts on the material in Ω.

The local/nonlocal distinctions drawn can be given a mechanical interpretation. This force is nonlocal precisely because material inside and outside of Ω interacts. In contrast, the classical theory of elasticity restricts the force interaction to the surface of Ω. The peridynamic global balance of angular momentum is

$$\int_{\Omega}\mathbf{y}\times\rho(\mathbf{x})\ddot{\mathbf{u}}(\mathbf{x},t)\,d\mathbf{x}=\int_{\Omega}\int_{\mathcal{B}}\mathbf{y}\times\mathbf{k}(\mathbf{y}'-\mathbf{y},\mathbf{x}',\mathbf{x})\,d\mathbf{x}'\,d\mathbf{x}+\int_{\Omega}\mathbf{y}\times\mathbf{b}(\mathbf{x},t)\,d\mathbf{x}\tag{5}$$

for $\Omega\subset\mathcal{B}$. The first term on the righthand side of (5) represents the torque of Ω, and may be replaced by $\int_{\Omega}\int_{\mathcal{B}/\Omega}\mathbf{y}\times\mathbf{k}(\mathbf{y}'-\mathbf{y},\mathbf{x}',\mathbf{x})\,d\mathbf{x}'\,d\mathbf{x}$ if and only if $\mathbf{k}(\mathbf{y}'-\mathbf{y},\mathbf{x}',\mathbf{x})$ is collinear with $\mathbf{y}'-\mathbf{y}$ as in bond-based peridynamics.

In classical elasticity, the locality of force interactions also implies that there is no length-scale independent of specific material behavior (e.g., outside of material inhomogeneities.) On the other hand, the nonlocal force density operator (1) does contain a length-scale, the peridynamic *horizon*—a nonzero volume over which material exerts forces. For instance, let the horizon be given by

$$\mathcal{H}(\mathbf{x}) = \{\mathbf{x}' \in \mathcal{B} \,|\, 0 \leq \|\mathbf{x}' - \mathbf{x}\| < \delta_{\mathbf{x}}\} \subset \mathcal{B}$$

so that the first terms on the righthand side of (5) and (4) are replaced with $\int_\Omega \int_{\mathcal{H}(\mathbf{x})} \mathbf{y} \times \mathbf{k}(\mathbf{y}' - \mathbf{y}, \mathbf{x}', \mathbf{x})\, d\mathbf{x}'\, d\mathbf{x}$ and $\int_\Omega \int_{\mathcal{H}(\mathbf{x})/\Omega} \mathbf{k}(\mathbf{y}' - \mathbf{y}, \mathbf{x}', \mathbf{x})\, d\mathbf{x}'\, d\mathbf{x}$, respectively, for $\Omega \subset \mathcal{H}(\mathbf{x})$. The horizon may vary with $\mathbf{x}$ and/or the forces about $\mathbf{x}$ so that the largest horizon over the body defines a maximum length scale.

The recently accepted paper [12] explains how the general state-based peridynamic material model converges to the classical elastic material model as the length scale, or horizon, vanishes, (assuming that the underlying deformation is sufficiently smooth). Building on the analysis of [12] and [11], a collapsed peridynamics stress tensor $\boldsymbol{\nu}^0(\mathbf{x}, t)$ is derived that is a function of the deformation gradient at $\mathbf{x}$ and so is a Piola-Kirchoff stress tensor. This limiting Piola-Kirchhoff stress tensor is differentiable and its divergence represents the force density due to internal forces. The limiting, or collapsed, stress-strain model satisfies the conditions in the classical theory for angular momentum balance, isotropy, objectivity, and hyperelasticity, provided the original peridynamic constitutive model satisfies appropriate conditions.

A body composed of discrete particles, e.g. atoms, can be represented as a peridynamic body. For example, suppose a set of discrete particles is given with reference positions $\mathbf{x}_i$ and masses m_i, $i = 1, 2, \ldots, n$. Let the force exerted by particle j on particle i after deformation of the system be denoted by $\mathbf{F}_{j,i}(t)$. Define a peridynamic body by $\rho(\mathbf{x}) = \sum_i m_i \delta(\mathbf{x} - \mathbf{x}_i)$ and $\mathbf{k}(\mathbf{y}' - \mathbf{y}, \mathbf{x}', \mathbf{x}) = \sum_i \sum_{j \neq i} \mathbf{F}_{j,i}(t) \delta(\mathbf{x}' - \mathbf{x}_j) \delta(\mathbf{x} - \mathbf{x}_i)$ for all $\mathbf{x}$, $\mathbf{x}'$ in $\mathbb{R}^3$, where $\delta(\mathbf{x})$ denotes the Dirac delta function or density (with units of per volume). Global conservation of linear momentum (4) where Ω is a volume enclosing only $\mathbf{x}_i$ reduces to

$$m_i \ddot{\mathbf{u}}(\mathbf{x}_i, t) = \sum_{j \neq i}^{n} \mathbf{F}_{j,i}(t), \qquad i = 1, 2, \ldots, n,$$

which is the familiar statement of Newton's second law in the particle mechanics setting. Replacing the Dirac delta densities with more general probability densities provides a mechanism for converting the set of discrete particles into a (continuum) peridynamics material model.

2.3. Discretization

Let $\mathbf{x}_1, \ldots, \mathbf{x}_n$ distinct points in $\mathcal{B}$ where $\mathcal{B} = \bigcup_{i=1}^n \Omega_i$ and $\mathbf{x}_i \in \Omega_i \subset \mathcal{H}(\mathbf{x}_i)$. The spatial discretization of (4) results in

$$\rho(\mathbf{x}_i) \ddot{\mathbf{u}}(\mathbf{x}_i, t) = \sum_{j \neq i} \mathbf{k}(\mathbf{y}_j - \mathbf{y}_i, \mathbf{x}_j, \mathbf{x}_i) V_j + \mathbf{b}(\mathbf{x}_i, t), \qquad i = 1, \ldots, n \tag{6}$$

where V_j is the volume of Ω_j. Note that the sum is not over $n - 1$ but rather over the number of $\mathbf{x}_j \in \mathcal{H}(\mathbf{x}_i)$. An advantage of quadrature based approaches is that they lead to three-dimensional, meshless Lagrangian implementations. A time integration scheme is then applied to (6), see [9, 13] for details. For a uniformly spaced $\mathbf{x}_i$, the midpoint quadrature rule gives a quadratic spatial rate of convergence. See [14, 15] for extensive verification studies in one and two dimensions (including adaptivity and comparisons with a commercial finite element code), respectively. The papers [16, 17] discuss the use of more sophisticated quadrature for the internal force calculation, and [18] discusses an implementation within an engineering finite element analysis code.

3. Applications

We review three successful multiscale applications of peridynamics within engineering analyses. All of the results discussed here were obtained with the Emu [9] or the molecular dynamics code LAMMPS [19, 13]. Both implementations are meshless three-dimensional Lagrangian codes—a mesh generator is not required. The examples (including validation where available) provide concrete evidence that peridynamics has been successfully used for three-dimensional engineering analyses that strain, perhaps go beyond, the limits of classical elasticity, by exploiting the nonlocality of force central to peridynamics. This nonlocality allows peridynamics to model complex material behavior possessing an intrinsic length-scale. The three applications presented deal with fracture problems—a quintessential multiscale phenomena. A compelling advantage of peridynamics is the ability to deal with fracture in a straight-forward fashion. This is accomplished by allowing bonds (e.g. between $\mathbf{x}'$ and $\mathbf{x}$) to break when stretched beyond some predetermined limit (see [9, 13] for a discussion) so enabling cracks initiate and propagate when and where is energetically favorable—unguided crack growth and complex interaction among cracks is the rule. This is in contrast to standard fracture mechanics approaches, see [20] for a review. The reader is referred to [21, 22] for applications of peridynamics not discussed in our paper.

3.1. Polycrystal fracture

Brittle fracture is a catalyst for failure in ceramic materials subject to appropriate mechanical loading. In order to predict the performance and structural integrity of ceramics, a fundamental understanding of brittle fracture in polycrystalline ceramics at the grain-size level is required. Such an understanding can then be used to design advanced structural ceramic systems with increased impact resistance, higher thermal shock resilience, etc. Here we present a novel approach for simulating fracture in polycrystalline ceramics, which has been difficult to do in the past, due to, in no small measure, the complexity of the phenomenon.

Combined transgranular (cracks pass through the grains) and intergranular (cracks propagate between the grains) fracture can take place in brittle fracture of ceramics. A transition between the trans- and inter-granular fracture is observed under certain loading. Experiments reported in [23] show that, while the main fracture mode is intergranular, local transgranular fracture also appears due to existence of crystalline phase at grain junctions. In addition, crack deflection and crack bridging mechanisms were observed due to the presence of rod-like grains. Further evidence of the importance of accurate modeling of inter- and trans-granular fracture in polycrystalline ceramics is presented in [24].

Existing models for simulating brittle fracture in polycrystalline ceramics that can include combined trans- and inter-granular crack propagation have severe limitations, including: the inability of modeling propagating cracks that naturally coalesce and/or branch; limitation to modeling only a single or a small number of cracks; complicated algorithms that cannot extend to three dimensions, etc.

The finite element method applied to equations of classical elasticity has been the preferred tool used in numerical models of polycrystalline materials (see [25, 26, 27, 28]). Fracture in polycrystalline materials has been modeled using cohesive-zone models initiated in [29, 30, 31]. Recently, some difficulties regarding time discontinuities in cohesive zone models have been pointed out in [32]. Bias of the crack propagation path and possible remedies are discussed in [33]. Mathematical and physical limitations, and constraints on cohesive laws are discussed in [34]. The most common approach for simulating brittle fracture of polycrystalline ceramics is to consider *only* intergranular fracture: cracks are restricted to grain boundaries (see, e.g., [35, 36, 37], finite elements with a "soft-kill method" are used to propagate the crack along grain boundaries instead of using a cohesive zone model. Lattice spring models have been used to study brittle fracture and damage in polycrystalline materials by, for example, [38, 39]. A

transition from intergranular to transgranular fracture with increasing grain boundary toughness is observed in [38], however, these studies are limited to 2D quasi-static analysis.

Compared to the methods discussed above, peridynamics for analyzing crack initiation, propagation, and fragmentation in a rate-dependent mechanically loaded Voronoi polycrystalline ceramics has important advantages. These include inter- and transgranular fracture are direct consequences of the computations and they do not have to be postulated via ad hoc assumptions as is the case for the classical approach; mode-transition and mode-mixing of crack propagation is naturally captured by the peridynamic formulation; fracture at triple-junction points is not controlled by ad-hoc assumptions but by the actual loading conditions in a region surrounding the triple-junctions; the meshfree discretization of peridynamics eliminates the need for complicated meshing algorithms for Voronoi polycrystals that represents an impediment to three dimensional computations.

We now summarize some results for simulating polycrystalline fracture in silicon ([40] will contain more details). Single-crystal silicon has a cubic structure, with the elastic moduli $c_{11} = 166$ GPa, $c_{44} = 80$ GPa, and $c_{12} = 64.5$ GPa. Extensions to other types of crystals is immediate and do not require special considerations. We generate a Voronoi polycrystal over a square with dimensions of 1cm by 1cm. Using 120 randomly distributed x and y coordinates for the Voronoi cells seeds, we obtain a grain-size distribution that is close to a Weibull distribution. This number of cells in the Voronoi structure gives the same grain-size distribution for different realizations (see [40]). For each Voronoi cell we assign a certain, random, orientation angle (from a uniform distribution). We define the micro-stiffness for the peridynamic bonds to vary with their orientation inside the grain and match the effective stiffness. Thus, the micro-stiffness depends on the orientation of each grain and the orientation of the bond inside the grain.

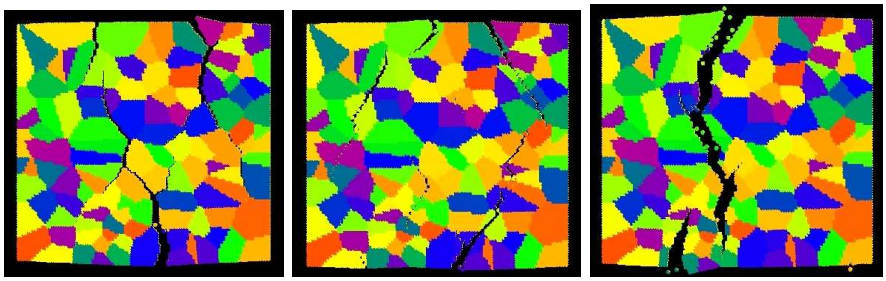

Figure 1. Fracture dependence on parameter β: β=0.25 (left), β=1 (center), and β=4(right).

The peridynamic bond relative elongation is given by s defined in (2), and the critical relative elongation at which a bond breaks is associated with the fracture energy and the peridynamic horizon via (see [9]) $s_0 = \sqrt{(5G_0)/(9\kappa\delta)}$, where G_0 is the material's (single crystal silicon) fracture energy and κ is the bulk modulus. Bonds that connect different grains have special properties that may be related to the properties of the grain boundaries. We select the micro-stiffness for such bonds to be the average of the corresponding directions in the two grains. For the critical relative elongation of the bonds that have ends in different grains we define an "interface strength coefficient" $\beta = s_0^{\mathrm{GB}}/s_0$ where s_0^{GB} is the critical relative elongation of the bonds that pass over a grain boundary, and s_0 is the value defined above for the single-crystal material. As we vary β from sub-unitary to super-unitary numbers, we change the strength of the grain boundaries from lower than the single crystal to higher than the single crystal.

The tests are performed using EMU [9] on a two dimensional grid of 100 nodes in each direction. Extensions to three dimensional simulations are immediate and does not require special considerations (except for the increased computer storage and floating point computation). We apply velocity boundary conditions on two sides for stretching along the

horizontal direction. The top and the bottom sides are free. The applied strain rate is constant equal to 50/s and the initial velocity distribution is consistent with this strain rate. We simulate 32 μs to reach an effective strain of 0.2%. We do not introduce initial cracks.

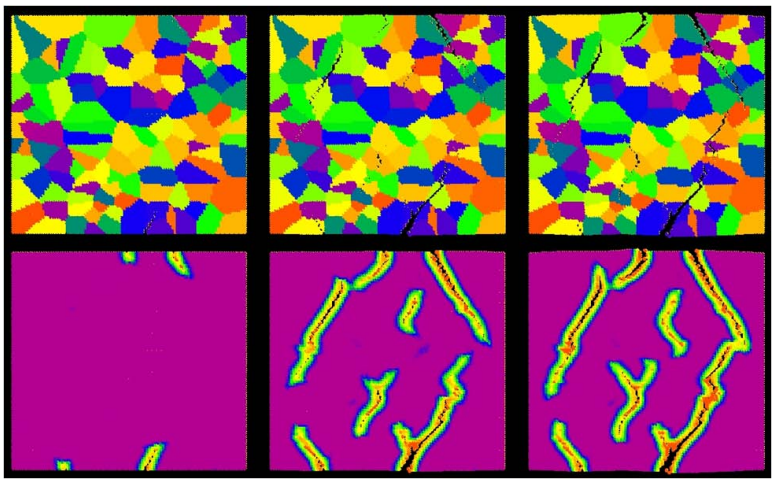

Figure 2. Evolution of damage and cracks in time for the $\beta = 1$ case. The top and bottom rows show the polycrystals boundaries and damage indices, respectively.

The plots in Fig. 1 show the polycrystal after 22 μs of the simulation for different values of the interface strength coefficient β. As β increases from 0.25 (left figure) to 1 (center) to 4 (right figure), we transition between purely intergranular fracture to pure transgranular fracture, passing through combined trans- and inter-granular fracture observed for average values of β. To better observe the ability of the peridynamic method to simulate crack propagation and crack interaction in polycrystalline ceramics we monitor the damage time-evolution for the case when $\beta = 1$ (see Fig. 2). We note that there are cracks that begin from the top and bottom edges, but also cracks that start in the interior of the sample, grow, branch, and finally join together.

3.2. Composite fracture and failure

The prediction of the spontaneous formation of a crack and its subsequent growth in load-carrying structures such as the wing or fuselage of an airplane presents a long-standing problem in computational solid mechanics. In a complex loading situation such as a bird strike, multiple cracks may occur simultaneously and interact. The path along which a crack propagates in a three dimensional structure is generally not known in advance and must be determined as part of the solution of a computer simulation, and ultimately depends on the underlying material. Recently anisotropic composite materials (such as CFRP) are replacing more traditional isotropic materials (such as high strength aluminum alloys) in part because of their larger specific strength promises significant weight savings. A typical composite material used within the aircraft industry is called "prepreg" and consists of individual plies stacked on top of each other and bonded together in an autoclave oven. Each ply consists of extremely stiff fibers that are embedded in a relatively soft matrix. Such a material exhibits many different failure mechanisms that can be active at the same time: delamination of adjacent plies or microbuckling of individual fibers are examples of common failure mechanisms in composites that have no counterpart in metals. Resolving the myriad failure mechanisms is essential in a simulation so that the correct path along which a crack propagates is computed. Peridynamics is ideally suited for describing damage propagation in composite materials because of (a) the ability to handle crack propagation when the crack path is not known a priori, (b) the natural

correspondence between fibers and peridynamic bonds, (c) the (infinitely) larger number of degrees of freedom in a peridynamic deformation state (in comparison to the classical local deformation gradient) that can capture a greater range of failure phenomena.

Anisotropy is introduced by allowing bonds in different directions to have different stiffness and failure properties. In the peridynamic model of a unidirectional fiber-reinforced lamina, the bonds in the direction of the fibers represent the fiber properties, while the bonds in all other directions represent the matrix properties. The fiber and matrix bonds have properties that are independent of each other, including both elastic response and failure properties.

The peridynamic model of a lamina is illustrated in Figure 3. The stiffness of matrix and fiber bonds, c^m, c^f, are chosen to match the effective laminate stiffness E_{11} and E_{22}. The critical strains for bond breakage in tension, s_0^{mt} and s_0^{ft}, are used to match the critical failure strains in a 0 and 90 degree lamina. In compression, the matrix and fiber bonds are assumed to fail at the same critical strain, denoted s_0^c. This assumption is made because the microbuckling mechanism for lamina failure in compression involves simultaneous localization in both the resin and fibers; hence it is not possible to identify separate failure criteria for each in compression. A model of a laminate is constructed from a stack of lamina models, each with a particular fiber direction. The laminas interact with each other through special peridynamic bonds that capture the through thickness stiffness E_{33} as well as the interlayer shear stiffness G_{13} and the corresponding energy release rates for mode I and II that can be measured in an DCB and ENF tests. For more detailed descriptions see [41, 42, 43, 44].

Using this simple model, a wide variety of problems involving damage propagation in CFRP panels were studied. Figure 4 shows a stiffened notched composite panel under compressive loading. Only half of the panel is shown due to symmetry. Note that in addition to the notch in the skin, the middle stringer has also been cut. The aim of such as simulation is to predict the damage tolerance capabilities in an lower wing structure of a composite airplane.

3.3. Nanofiber networks

There is much interest in polymer nanofibers because of their desirable structural mechanical properties. In particular, they possess a large surface area to volume ratio, as well as high axial strength and extreme flexibility. The use of nanofibers is being explored in such diverse areas as composites, protective clothing, catalysis, electronics, biomedicine (including tissue engineering, implants, membranes, and drug delivery), filtration, and agriculture [45]. Recently, polymer nanofibers have also been proposed as a filters for chemical warfare defense [46]. The ability to tailor the properties of nanofiber networks and membranes for specific applications requires that an understanding of the mechanical properties of these networks and membranes through modeling and simulation. A peridynamic model for simulation of the mechanical behavior and strength and toughness properties of three-dimensional nanofiber networks under imposed stretch deformation was proposed in [47].

In this numerical model, the peridynamic prototype microelastic brittle (PMB) [9] was augmented with a Lennard-Jones potential to mimic the effects of van der Waals forces. This augmented potential was applied to nanofiber networks similar to that shown in Figure 5(a). The model domain is 400 nm wide by 400 nm high by 10 nm thick. The top, bottom, left, and right ends have a constant velocity boundary condition applied to induce a biaxial strain that eventually leads to the failure of the nanofiber network. Simulations performed with the PDLAMMPS code [13] are shown in Figure 5. Detailed numerical simulation in [47] led to the observations that van der Waals interactions are important in increasing the strength and toughness of the nanofiber network, and that heterogeneity in the strength of bonds in the nanofiber network can increase its toughness and ductility. Additionally, reorientation due to breakage and deformation, and a Poisson effect due to van der Waals induced accretion, are the two main mechanisms that control the dynamic deformation and damage of nanofiber

networks [47].

[1] de Pablo J J and Curtin W A (eds) 2007 *Multiscale Modeling in Advanced Materials Research* (*MRS Bulletin* vol 32) (Material Research Society)
[2] Miller R E and Tadmor E B 2007 *Multiscale Modeling in Advanced Materials Research* (*MRS Bulletin* vol 32) ed de Pablo J J and Curtin W A pp 920–926
[3] Bažant Z P and Jirásek M 2002 *J. of Eng. Mech.* **128** 1119–1149
[4] Chen Y, Lee J D and Eskandarian A 2004 *Int. J. of Solids and Structures* **41** 2085–2097
[5] Eringen A C 2002 *Nonlocal continuum field theories* (Springer-Verlag NewYork, Inc)
[6] Silling S A 2000 *J. Mech. Phys. Solids* **48** 175–209
[7] Silling S A, Epton M, Weckner O, Xu J and Askari E 2007 *J. Elasticity* **88** 151–184
[8] Weckner O and Abeyaratne R 2005 *J. Mech. Phys. Solids* **53** 705–728
[9] Silling S A and Askari E 2005 *Comp. Struct.* **83** 1526–1535 EMU available at `www.sandia.gov/emu/emu.htm`
[10] Ciarlet P 1988 *Finite Element Method for Elliptic Problems* (North-Holland, Amsterdam)
[11] Lehoucq R B and Silling S A 2008 *J. Mech. Phys. Solids* **56** 1566–1577
[12] Silling S A and Lehoucq R B 2008 *J. Elasticity* Article in Press, available online
[13] Parks M L, Lehoucq R B, Plimpton S J and Silling S A 2008 *Comp. Phys. Comm.* Article in Press, available online
[14] Bobaru F, Yang M, Alves L F, Silling S A, Askari A and Xu J 2008 *Int. J. Num. Meth. Eng.* Submitted
[15] Bobaru F, Yang M, Alves L F, Silling S A, Askari A and Xu J 2008 *Int. J. Num. Meth. Eng.* In preparation
[16] Emmrich E and Weckner O 2007 *Math Mod Analysis* **12** 17–27
[17] Emmrich E and Weckner O 2005 *Math and Mech of Solids* **12** 363–384
[18] Macek R and Silling S 2007 *Fin. Elem. Anal. Design* **43** 1169–1178
[19] Plimtpon S J 1995 *J. Comp. Phys.* **117** 1–19 LAMMPS available at `http://lammps.sandia.gov`
[20] Ingraffea A R 2007 *Encyclopedia of Computational Mechanics* (*Solids and Structures* vol 2) ed Stein E, de Borst R and Hughes T J R (Wiley) chap 11
[21] Gerstle W, Sau N and Silling S 2007 *Nuc. Eng. Des* **237** 1250–1258
[22] Silling S A and Bobaru F 2005 *Int. J. Non-Linear Mech.* **40** 395–409
[23] Lee B T, Han B D and Kim H D 2003 *Materials Letters* **58** 74– 79
[24] Sun X, Li G J, Guo S, Xiu Z, Duan K and Hu X 2005 *J of the American Ceramic Society* **88** 1536–1543
[25] Ghosh S and Mukhopadhyay S 1993 *Comp Meth Appl Mech Eng* **104** 211–247
[26] Ghosh S and Mallett R 1994 *Comp. Struct.* **50** 33–46
[27] Zavattieri P, Raghuram P and Espinosa H 2001 *J. Mech. Phys. Solids* **49** 27–68
[28] Zhang D, Wu M and Feng F 2001 *International Journal of Plasticity* **21** 801–834
[29] Barenblatt G 1959 *Applied Mathematics and Mechanics (PMM)* **23** 622636
[30] Dudgale D 1960 *J. Mech. Phys. Solids* **8** 100–104
[31] Barenblatt G 1962 *Advances in Applied Mechanics* **7** 55–129
[32] Papoulia K, Sam C and Vavasis S 2003 *Int. J. Num. Meth. Eng.* **58** 679–701
[33] de Borst R 2003 *Eng. Frac. Mech.* **70** 1743–1757
[34] Jin Z and Sun C 2005 *Int. J. Frac.* **134**
[35] Grah M, Alzebdeh K, Sheng P, Vaudin M, Bowman K and Ostoja-Starzewski M 1996 *Acta Materialia* **44** 4003–4018
[36] Holm E 1998 *Journal of the American Ceramic Society* **81** 455–459
[37] Maiti S, Rangaswamy K and Geubelle P 2005 *Acta Materialia* **53** 823 – 834
[38] Yang W, Srolovitz D, Hassold G and Anderson M 1990 *In Simulation and Theory of Evolving Microstructures* (The Metallurgical Society: Warrendale, PA) chap Microstructural effects in the fracture of brittle materials, pp 277–284
[39] Rinaldi A, Krajcinovic D, Peralta P and Lai Y C 2008 *Mechanics of Materials* **40** 17–36
[40] Bobaru F and Silling S 2008 *in preparation*
[41] Askari A, Xu J and Silling S A 2006 *Proc. 44th AIAA Aerospace Sciences Meeting and Exhibit* AIAA 2006-88 (Reno, NV)
[42] Silling S A, Askari A, Nelson K, Weckner O and Xu J 2008 *Proc. SAMPE Fall Technical Conference 2008*
[43] Xu J, Askari A, Weckner O and Silling S A 2008 *J. Aero. Eng.* Article in Press
[44] Xu J, Askari A, Weckner O, Razi H and Silling S A 2007 *Proc. 48th AIAA/ASME/ASCE/AHS/ASC Structures, Structural Dynamics, and Materials Conference* (Honolulu, HI)
[45] Dzenis Y 2004 *Science* **304** 1917–19
[46] Ramaseshan R, Sundarrajan S, Liu Y, Barhate R, Lala N L and Ramakrishna S 2006 *Nanotechnology* **17** 2947–2953
[47] Bobaru F 2007 *Modelling Simul. Mater. Sci. Eng.* **15** 397–417

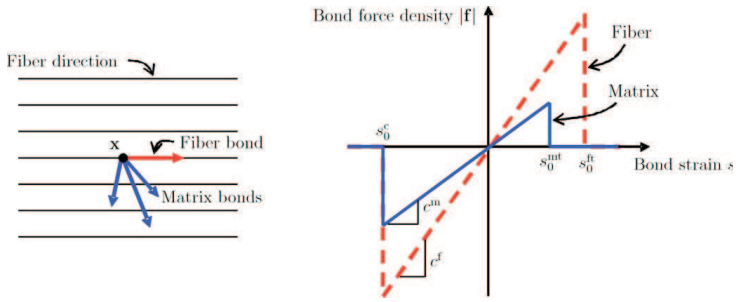

Figure 3. Peridynamic lamina model

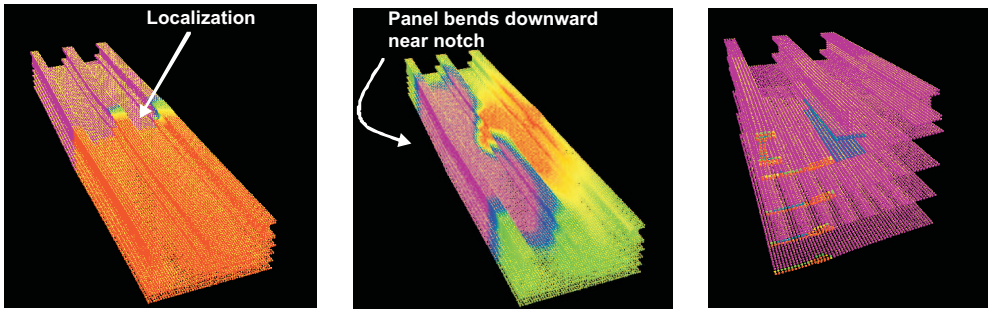

Figure 4. (Left to right) Axial displacement during damage growth; out of plane displacement growth; damage at a later time shows disbonding.

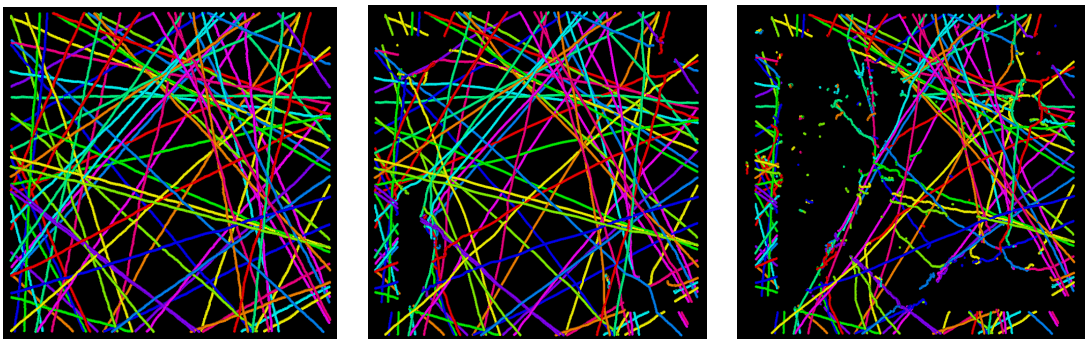

Figure 5. Peridynamic simulation of polymer nanofiber network under biaxial strain. (Left to right) Undeformed configuration; Biaxial strain of 17.6% (30 ns); Biaxial strain of 29.4% (50 ns). Colors indicate individual fibers.